Triggered Superradiance and Spin Inversion Storage in a Hybrid Quantum System

Wenzel Kersten[1,*] Nikolaus de Zordo,[1] Oliver Diekmann,[2] Tobias Reiter,[2] Matthias Zens,[2]
Andrew N. Kanagin,[1] Stefan Rotter,[2] Jörg Schmiedmayer,[1,†] and Andreas Angerer[1]

[1]*Vienna Center for Quantum Science and Technology, Atominstitut, TU Wien, Stadionallee 2, A-1020 Vienna, Austria*
[2]*Institute for Theoretical Physics, TU Wien, Wiedner Hauptstraße 8-10/136, A-1040 Vienna, Austria*

We study the superradiant emission of an inverted spin ensemble strongly coupled to a superconducting cavity. After fast inversion, we detune the spins from the cavity and store the inversion for tens of milliseconds, during which the remaining transverse spin components disappear. Switching back on resonance enables us to study the onset of superradiance. A weak trigger pulse of a few hundred photons shifts the superradiant burst to earlier times and imprints its phase onto the emitted radiation. For long hold times, the inversion decreases below the threshold for spontaneous superradiance. There, the energy stored in the ensemble can be used to amplify microwave pulses passing through the cavity.

Superradiance is the process by which an ensemble of excited two-level systems synchronizes to produce a short, highly coherent burst of light [1]. The buildup of correlations during the collective decay, mediated by an enhanced coupling to a common mode, gives rise to nonlinear scaling of the decay rate with the number of emitters [2]. Superradiant (SR) emission is not only fundamental to many fields of physics, but also attracts increasing interest for applications in metrology [3], laser physics [4–6], and quantum technology in general [7–13]. SR phenomena are at the heart of the transition from a genuine quantum regime, where individual fluctuations of the vacuum field will jump start the collective decay of inverted emitters, to the classical regime, where the emission is akin to that of a macroscopic radiating dipole.

Whereas experiments on superradiance have recently been successfully transferred from atomic ensembles to solid-state spin systems [14,15], the possibilities this opens up for controlling and exploiting superradiance for applications have been very little explored so far. Progress in this direction has primarily been hindered by the fact that systems giving rise to superradiance are fundamentally unstable, reacting to the slightest disturbance. While this extreme sensitivity even to weak signals poses a great challenge for experimental implementation, it also provides potential avenues for applications in sensor and detector technology [3,16].

Our work is enabled by an experimental platform that allows us (i) to invert a large ensemble of nitrogen-vacancy (NV) spins, and (ii) to hold and stabilize the stored inversion for up to 20 ms—4 orders of magnitude longer than the timescale of the SR emission. Stabilization is achieved by rapidly detuning the spins from cavity resonance after their inversion, switching off the interaction with the mode. This allows us to study and control the emission of a SR burst that releases the energy stored in the ensemble. We employ weak microwave (MW) pulses to trigger the SR emission and also explore a regime with reduced inversion, where the spins act as a gain medium.

Our resonator [see Fig. 1(a)] is based on two opposing superconducting chips that exhibit a small mode volume with homogeneous coupling strength, while retaining a high quality factor of $Q \approx 3000$. This design allows us (i) to reach the regime of strong collective spin-cavity coupling already with a number of NVs that is reduced by 3 orders of magnitude and (ii) to add a small loop of superconducting wire which enables magnetic tuning of the spins in and out of the cavity resonance faster than the SR timescale. Previous cavity realizations for this type of SR system [22,23] would resist a sudden field change due to induced currents in their bulk structures.

The two sapphire chips with a 200 nm thin layer of $16 \times 16 \text{ mm}^2$ niobium are mounted in a copper housing. The identical patterns on both chips feature a hole in the center from which a 4 μm slit reaches outward, resembling a split ring resonator [24]. The chips are stacked, with the roughly cube-shaped diamond sample placed between the center holes. The hole radii, the distance between the chips, and the sample size are all of similar dimension $d \sim 200$ μm. This configuration results in a resonance frequency of $\omega_c/2\pi = 3.105$ GHz and a linewidth of $\kappa/2\pi = 0.51$ MHz (HWHM).
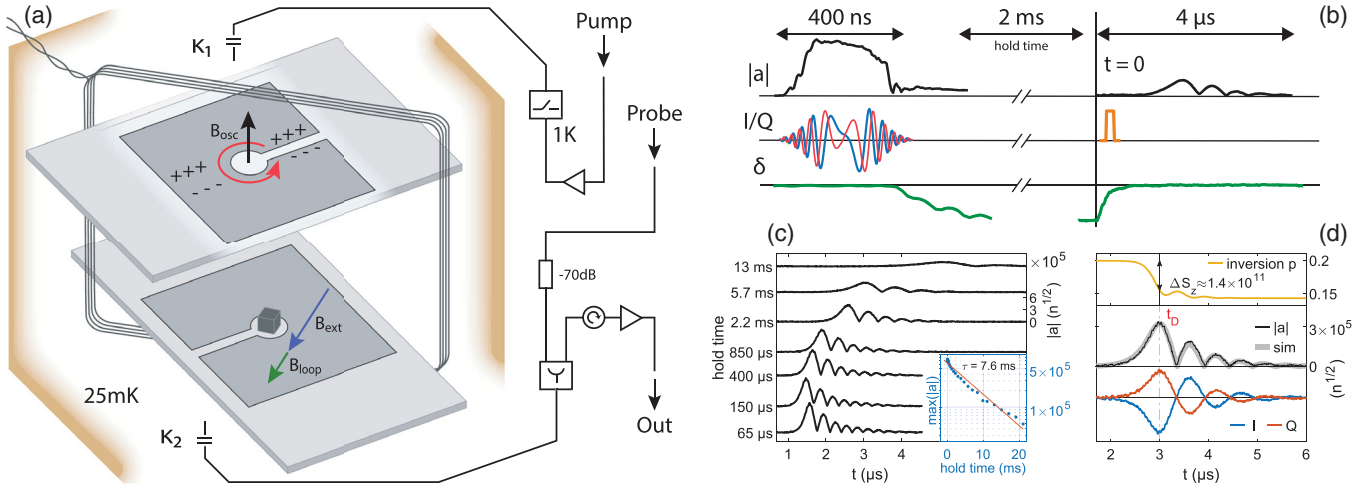
FIG. 1. (a) Schematic of the MW cavity located in a dilution refrigerator at 25 mK and connected to a homodyne MW setup. Two sapphire chips with opposing split ring structures and the diamond sample are stacked inside a copper box. Between the center holes the oscillating magnetic field homogeneously penetrates the sample. A superconducting wire loop wrapped around the chips enables rapid spin detuning. Port 1 is connected to the pump line, which can be decoupled at the 1 K stage using a solenoid switch for noise suppression. Port 2 is connected to the out line for acquiring data, and the attenuated probe line for injecting weak trigger pulses. (b) Experiment sequence: we use a modified chirp pulse (red and blue) to invert the spin ensemble and subsequently modulate the spin detuning δ to store the inversion. After a variable hold time we bring the spins back into resonance and measure the cavity amplitude $|a|$ of the SR decay, optionally triggered by a short probe pulse (orange). (c) SR decays for varying hold times, triggered by the pump-line amplifier noise. The inset shows the SR decay maxima with an exponential fit in a semilog plot. (d) Example data and simulation of an SR decay and its quadratures I/Q, with simulated inversion p. The vertical line indicates t_D, the time of maximum cavity amplitude. The number of cavity photons $n = |a|^2$ (calibration in Supplemental Material [17]) agrees well with the estimated number of decaying spins ΔS_z.

The resonator couples homogeneously to all spins with a single spin coupling strength of $g_0 \approx 2$ Hz, resulting in a collective coupling of $g_{\mathrm{coll}}/2\pi = 5.17$ MHz for a total number of spins of $N \approx 6.4 \times 10^{12}$. The spin system's coherent response is determined by the effective ensemble linewidth of $\Gamma_\perp/2\pi = 4.27$ MHz [25], combining the inhomogeneously broadened spin frequency distribution [26] and the individual spin's linewidth of $\gamma_\perp/2\pi \approx 208$ kHz [27]. More details on the resonator and theoretical treatment can be found in Supplemental Material [17]. The resulting cooperativity parameter of our coupled system is $C = g_{\mathrm{coll}}^2/(\kappa\Gamma_\perp) \approx 12.2$.

To begin our explorations, we magnetically tune all 4 NV subensembles into resonance with the cavity using a static vector field and a loop current of 1 A. The NVs are initially prepared in a state close to the ground state and act as effective two-level systems. Next, we use a 400 ns modified chirp pulse with a Gaussian envelope to invert the spins. We then rapidly switch off the loop current in about 200 ns using a semiconductor switch, detuning the spins by $\delta/2\pi \approx 26$ MHz for a given hold time. This detuning by more than the ensemble linewidth inhibits the SR interaction of the spin ensemble with the cavity mode [25], thereby storing the inversion. Initially, the stored population in the upper spin state is $\approx 67\%$. For details of the initialization see Supplemental Material [17].

During the hold time, the remaining transversal component of the collective spin vector $S_- = S_x - iS_y$, which initially persists after the creation of the partially inverted state, undergoes dephasing and is effectively eliminated. When tuning the ensemble back into resonance, we thus create a metastable inverted state whose tipping angle $\theta = \arctan(|S_-|/S_z)$ with respect to the z axis in the Bloch sphere is exponentially decreased for longer hold times. If the product of the stored ensemble inversion $-1 \leq p \leq +1$ and cooperativity is above the threshold $pC > 1$, this metastable state will become unstable and decay by emitting a SR photon burst, as shown in [25]. Here, the inversion parameter p is implicitly defined by $S_z = \frac{1}{2}\langle \sum_j \sigma_z^j \rangle = pN/2$. In this state, the presence of even a single photon in the cavity will stimulate the collective emission of radiation, starting a self-accelerating photonic avalanche. During this process, the energy released in the form of cavity photons gradually builds up, reaches a maximum, and then oscillates back and forth between the two subsystems, before the process stops due to the dephasing of the spins and their decoherence. The full experimental sequence is summarized in Fig. 1(b).

Our first notable result is presented in Fig. 1(c), where we plot the SR decay pulses for varying inversion hold times. Here, the SR decay is triggered by noise from the high power amplifier of the pump line. The measured SR
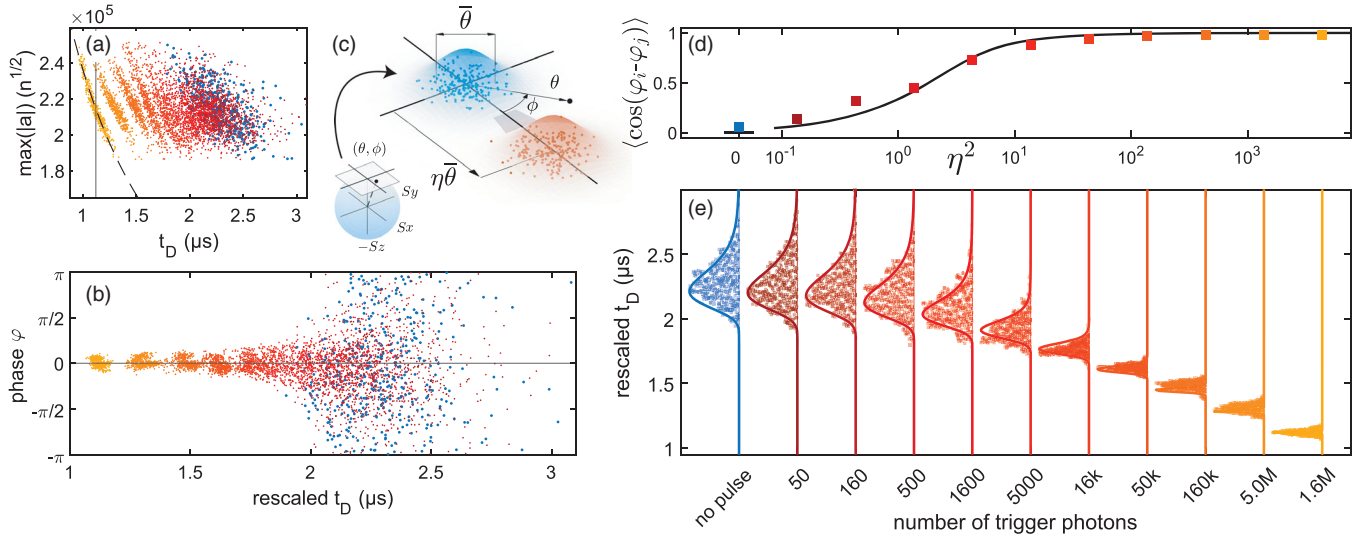
FIG. 2. Triggering the SR decay with 100 ns pulses containing different numbers of photons, color coded according to (e). (a) Maxima of the SR decay amplitudes plotted over delay times t_D. (b) Corresponding SR decay phases φ plotted over a rescaled t_D axis. The rescaled t_D values result from a transformation that aligns the dashed curve in (a) onto the vertical line. (c) Initial state of the collective spin vector with coordinates (θ, ϕ) close to the north pole of the Bloch sphere: in-plane distribution before (blue) and after (red) the coherent displacement η in units of the width $\bar{\theta}$ induced by the trigger pulse. (d) Phase average over all runs $\langle\cos(\varphi_i - \varphi_j)\rangle$ quantifying the phase randomness from the measured sets of φ. (e) Swarm plots of the delay time t_D data. The solid lines in (d) and (e) are obtained from our theoretical description, varying only the parameter η.

dynamics are captured in a semiclassical description using the Maxwell-Bloch equations [28]. We model the time evolution starting from an inverted state with a slight tipping angle accounting for fluctuations that initiate the SR decay (see Supplemental Material [17]). To simulate the measured signals of $|a|$ we only adjust the ensemble inversion p and a time offset, resulting in curves as shown in Fig. 1(d). The role of fluctuations at the start of the SR decay process is studied in more detail below. We find the decay maximum $\max(|a|)$, an indirect measure of the energy stored by the spins, to decrease roughly exponentially with increasing hold times, exhibiting a characteristic timescale of $\tau = 7.6$ ms [see inset Fig. 1(c)]. For hold times longer than 20 ms, the inversion has already decreased below the threshold $pC = 1$ for spontaneous superradiance. We propose two timescales for the relaxation of the inverted state. First, on a millisecond timescale, the ensemble is rapidly randomized due to spin-spin interactions involving NVs with short lifetimes (so called *fluctuators* [29]), acting as local sinks for the inversion via spin diffusion. Second, when $p = 0$ is reached, the ensemble relaxes to the ground state on a longer timescale, characterized by $T_1 = 134$ s (see Supplemental Material [17]).

We now focus on the onset of the SR decay process and the possibility to trigger it prior to its self-decay. Using a 2 ms hold time, we give the cavity mode enough time to reach thermal equilibrium after the inversion pulse and subsequent decoupling from the high power amplifier noise by the solenoid switch, with an estimated number of $\bar{n} \approx 3$

thermal photons remaining. The partially inverted state that is brought back into resonance has zero tipping angle apart from unavoidable quantum and thermal fluctuations. Another 150 ns after switching back the detuning current (defined as $t = 0$), we send a 100 ns trigger pulse through the highly attenuated MW probe line. The pulse is resonant with the cavity and contains a calibrated number of photons (see Supplemental Material [17]). The experiment is repeated many times for varying numbers of trigger photons, and without trigger pulse. For every run, we extract the delay time t_D and the I_D/Q_D quadrature values of the SR decay maximum [cf. Fig. 1(d)]. The SR decay amplitudes $\max(|a|) = \sqrt{I_D^2 + Q_D^2}$ show variations of $\pm 10\%$ between runs as visible in Fig. 2(a), mainly caused by the solenoid switch's latching mechanism. To clearly study the influence of the number of trigger photons on the delay times, we adjust for the expected systematic dependence of $t_D \propto \max(|a|)^{-1}$ and rescale the t_D data. The SR decay phases $\varphi = \arctan(Q_D/I_D)$ are independently corrected for a linear phase drift with t_D, caused by a minor constant detuning of the spins. Details of both methods are given in Supplemental Material [17]. The resulting sets of phases and rescaled delay times are presented in Figs. 2(b) and 2(e).

Clearly, stronger trigger pulses with higher numbers of photons n_{trig} lead to earlier t_D values and narrower distributions for t_D and φ. While our simulation allows us to describe the decay process starting from a slightly tipped initial collective spin vector, it is the randomness in the initial conditions that leads to the observed variance in

time and phase. These thermal and quantum fluctuations are not included in our semiclassical model. To understand the observed phenomena, we split the analysis of the SR decay into two stages [2,16,30].

The decay process starts with a linear stage, in which the (optional) trigger pulse leads to a coherent rotation of the collective spin vector about an axis defined by the phase of the pulse, which is kept identical for all runs. Prior to this rotation, the initial state is located very close to the $+z$ axis but with a small tipping angle $\theta = \arctan(|S_-|/S_z)$ and random polar angle $\phi = \arg(S_-)$. As $\cos\theta \simeq 1$ throughout the linear phase, we can treat the spin vector to be confined to a plane with a z offset corresponding to the initial inversion. The geometric construction of this plane is illustrated in Fig. 2(c), mathematical formulas of the distribution functions are given in Supplemental Material [17]. The initial state of the spin vector follows a two dimensional Gaussian distribution of width $\bar{\theta}$ centered at $\theta = 0$. The influence of the trigger pulse then causes a displacement in the plane, which we choose to be in the direction of $\phi = 0$. The parameter η expresses the displacement in units of the width parameter $\bar{\theta}$. For growing η, i.e., higher trigger pulse powers, the initially randomly distributed polar angles become increasingly well defined and approach a narrow distribution around $\phi = 0$ [see Fig. 2(b)].

After this linear stage, where the collective spin vector is coherently displaced from its random in-plane starting position, we enter a nonlinear regime. Now the SR dynamics dominate and via a collective process of stimulated emission the spin vector accelerates its rotation toward the equator while emitting a considerable burst of MW radiation.

The phase φ of the emitted decay pulse is directly determined by the value of ϕ at the start of the nonlinear stage. Less directly, we can infer the initial tipping angles θ from the delay times t_D, which result via the relation $t_D = -2T_R \log(\theta/2)$ [16]. Here, the parameter T_R represents the timescale for the SR emission process (see Supplemental Material [17]). With this relation, and the displaced Gaussian distribution that describes θ and ϕ depending on η [see Fig. 2(c)], we can reproduce the t_D data in Fig. 2(e) and the phase randomness quantified by $\langle\cos(\varphi_i - \varphi_j)\rangle$ [16] in Fig. 2(d). To this end, we fix the values of the SR timescale $T_R = 142$ ns and width of the Gaussian $\bar{\theta} = 5.85 \times 10^{-4}$, and vary only η.

As the displacement η is caused by the MW magnetic field of the trigger pulse, its square is a measure of the energy imparted onto the spin system during the linear stage of the SR process. We can therefore use the x axes in both Figs. 2(d) and 2(e) interchangeably, confirming $n_{\mathrm{trig}} \propto \eta^2$. Remarkably, a weak MW pulse on the order of 10^{-11} photons per spin is sufficient to have an observable effect on the SR decay. By reducing the number of spins
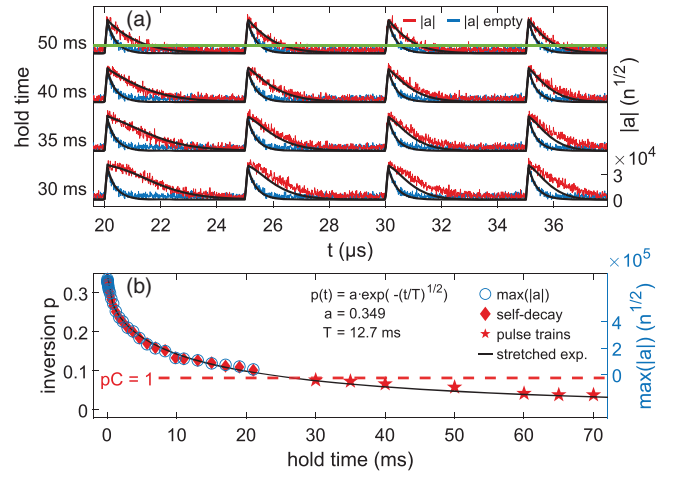
FIG. 3. (a) Cavity amplitude $|a|$ for a series of 100 ns pulses, each injecting $n_{\mathrm{trig}} \approx 1.5 \times 10^9$ photons, amplified by the partially inverted spin ensemble in the reduced effective cooperativity regime $pC < 1$ for different hold times (red). In comparison, we plot the signal obtained with an empty cavity where spins are far detuned (blue). For choosing the parameters in our semiclassical model (black), we ignore noise below a certain threshold (green line at the top). (b) Ensemble inversion as a function of hold time, extracted by simulations in the two regimes above and below $pC = 1$. Above this threshold, the pulse maxima (right y axis) follow the values of p from simulations of the self-decays shown in Fig. 1(c). A stretched exponential with exponent $1/2$ (characteristic for spin diffusion in three dimensions [29]) is fitted to the inversion.

while maintaining a high cooperativity, the sensitivity to both amplitude and phase could be further enhanced.

We now investigate a regime of reduced effective cooperativity $pC < 1$, where SR emission does not occur spontaneously [25]. To that end, we employ hold times longer than 20 ms, thus reducing the polarization below the threshold for the SR decay. We probe the system by injecting, at 5 μs intervals, a sequence of resonant MW pulses of 100 ns duration via the pump line. Interestingly, in Fig. 3(a), we find that this results in an amplification of the pulses as compared to the empty cavity response (with far detuned spins). Although no spontaneous SR decay occurs on its own, it is still possible to repeatedly extract energy from the stored inversion. The incident pulses hereby effectively supply the necessary coherence that is otherwise constituent to the SR emission, but hindered from building up when the stored inversion is insufficient. Notably, tens of injected MW pulses can be amplified in succession (see Supplemental Material [17]). We are able to replicate the measured dynamics using our numerical model with only the amplitude of the incident pulses (kept fixed for all fits) and the ensemble inversion p as free parameters. These results are combined in Fig. 3(b) with the p values attained by simulating the SR self-decays [cf. Fig. 1(d)]. The semiclassical model seamlessly captures the behavior of

our system in both regimes of high and low effective cooperativity.

In summary, we present an experimental platform to store the energy of an inverted spin ensemble for tens of milliseconds and to release it in a strong SR burst. By initializing the system to a fully upright inverted state, we demonstrate a high sensitivity to weak MW pulses that strongly influence the subsequent SR dynamics via both amplitude and phase of the trigger pulse. The decrease of inversion over time lets us explore a regime of reduced cooperativity without spontaneous SR emission, where the inverted spins effectively act as a gain medium for a series of short MW pulses. Our observations provide insight into the collective behavior of inverted spin systems and its experimental control.

---

*Corresponding author.
 wenzel.kersten@tuwien.ac.at
†Corresponding author.
 hannes-joerg.schmiedmayer@tuwien.ac.at

[1] R. H. Dicke, Coherence in spontaneous radiation processes, Phys. Rev. **93**, 99 (1954).

[2] M. Gross and S. Haroche, Superradiance: An essay on the theory of collective spontaneous emission, Phys. Rep. **93**, 301 (1982).

[3] M. Koppenhöfer, P. Groszkowski, H.-K. Lau, and A. A. Clerk, Dissipative superradiant spin amplifier for enhanced quantum sensing, PRX Quantum **3**, 030330 (2022).

[4] J. G. Bohnet, Z. Chen, J. M. Weiner, D. Meiser, M. J. Holland, and J. K. Thompson, A steady-state superradiant laser with less than one intracavity photon, Nature (London) **484**, 78 (2012).

[5] Y. Zhang, C. Shan, and K. Mølmer, Ultranarrow Superradiant Lasing by Dark Atom-Photon Dressed States, Phys. Rev. Lett. **126**, 123602 (2021).

[6] Q. Wu, Y. Zhang, X. Yang, S.-L. Su, C. Shan, and K. Mølmer, A superradiant maser with nitrogen-vacancy center spins, Sci. China Phys. Mech. Astron. **65**, 217311 (2022).

[7] A. Kuzmich, W. Bowen, A. Boozer, A. Boca, C. Chou, L.-M. Duan, and H. Kimble, Generation of nonclassical photon pairs for scalable quantum communication with atomic ensembles, Nature (London) **423**, 731 (2003).

[8] D. Yang, S.-h. Oh, J. Han, G. Son, J. Kim, J. Kim, M. Lee, and K. An, Realization of superabsorption by time reversal of superradiance, Nat. Photonics **15**, 272 (2021).

[9] J. Kim, D. Yang, S.-h. Oh, and K. An, Coherent single-atom superradiance, Science **359**, 662 (2018).

[10] R. Pennetta, D. Lechner, M. Blaha, A. Rauschenbeutel, P. Schneeweiss, and J. Volz, Observation of Coherent Coupling Between Super- and Subradiant States of an Ensemble of Cold Atoms Collectively Coupled to a Single Propagating Optical Mode, Phys. Rev. Lett. **128**, 203601 (2022).

[11] M. O. Araújo, I. Krešić, R. Kaiser, and W. Guerin, Super-radiance in a Large and Dilute Cloud of Cold Atoms in the Linear-Optics Regime, Phys. Rev. Lett. **117**, 073002 (2016).

[12] J. Kim, S.-h. Oh, D. Yang, J. Kim, M. Lee, and K. An, A photonic quantum engine driven by superradiance, Nat. Photonics **16**, 707 (2022).

[13] A. Sherman, O. Zgadzai, B. Koren, I. Peretz, E. Laster, and A. Blank, Diamond-based microwave quantum amplifier, Sci. Adv. **8**, eade6527 (2022).

[14] A. Angerer, K. Streltsov, T. Astner, S. Putz, H. Sumiya, S. Onoda, J. Isoya, W. J. Munro, K. Nemoto, J. Schmiedmayer et al., Superradiant emission from colour centres in diamond, Nat. Phys. **14**, 1168 (2018).

[15] J. Q. Quach, K. E. McGhee, L. Ganzer, D. M. Rouse, B. W. Lovett, E. M. Gauger, J. Keeling, G. Cerullo, D. G. Lidzey, and T. Virgili, Superabsorption in an organic microcavity: Toward a quantum battery, Sci. Adv. **8**, eabk3160 (2022).

[16] P. Goy, L. Moi, M. Gross, J. M. Raimond, C. Fabre, and S. Haroche, Rydberg-atom masers. II. Triggering by external radiation and application to millimeter-wave detectors, Phys. Rev. A **27**, 2065 (1983).

[17] See Supplemental Material at http://link.aps.org/supplemental/10.1103/PhysRevLett.131.043601 for further details on the experimental system and theoretical treatment, which includes Refs. [18–21].

[18] S. O. Rice, Mathematical analysis of random noise, Bell Syst. Tech. J. **24**, 46 (1945).

[19] E. A. Cooper and H. Farid, A toolbox for the radial and angular marginalization of bivariate normal distributions, arXiv:2005.09696.

[20] C. Gardiner and P. Zoller, Quantum Noise: A Handbook of Markovian and Non-Markovian Quantum Stochastic Methods with Applications to Quantum Optics (Springer Science & Business Media, New York, 2004).

[21] T. Astner, J. Gugler, A. Angerer, S. Wald, S. Putz, N. J. Mauser, M. Trupke, H. Sumiya, S. Onoda, J. Isoya et al., Solid-state electron spin lifetime limited by phononic vacuum modes, Nat. Mater. **17**, 313 (2018).

[22] A. Angerer, T. Astner, D. Wirtitsch, H. Sumiya, S. Onoda, J. Isoya, S. Putz, and J. Majer, Collective strong coupling with homogeneous Rabi frequencies using a 3D lumped element microwave resonator, Appl. Phys. Lett. **109**, 033508 (2016).

[23] J. R. Ball, Y. Yamashiro, H. Sumiya, S. Onoda, T. Ohshima, J. Isoya, D. Konstantinov, and Y. Kubo, Loop-gap microwave resonator for hybrid quantum systems, Appl. Phys. Lett. **112**, 204102 (2018).

[24] W. Hardy and L. Whitehead, Split-ring resonator for use in magnetic resonance from 200–2000 MHz, Rev. Sci. Instrum. **52**, 213 (1981).

[25] B. Julsgaard and K. Mølmer, Dynamical evolution of an inverted spin ensemble in a cavity: Inhomogeneous broadening as a stabilizing mechanism, Phys. Rev. A **86**, 063810 (2012).

[26] K. Sandner, H. Ritsch, R. Amsüss, C. Koller, T. Nöbauer, S. Putz, J. Schmiedmayer, and J. Majer, Strong magnetic coupling of an inhomogeneous nitrogen-vacancy ensemble to a cavity, Phys. Rev. A **85**, 053806 (2012).

[27] S. Putz, A. Angerer, D. O. Krimer, R. Glattauer, W. J. Munro, S. Rotter, J. Schmiedmayer, and J. Majer, Spectral hole burning and its application in microwave photonics, Nat. Photonics **11**, 36 (2017).

[28] H. J. Carmichael, *Statistical Methods in Quantum Optics 1: Master Equations and Fokker-Planck Equations* (Springer Science & Business Media, New York, 1999), Vol. 1.

[29] J. Choi, S. Choi, G. Kucsko, P. C. Maurer, B. J. Shields, H. Sumiya, S. Onoda, J. Isoya, E. Demler, F. Jelezko, N. Y. Yao, and M. D. Lukin, Depolarization Dynamics in a Strongly Interacting Solid-State Spin Ensemble, Phys. Rev. Lett. **118**, 093601 (2017).

[30] L. Moi, P. Goy, M. Gross, J. M. Raimond, C. Fabre, and S. Haroche, Rydberg-atom masers. I. A theoretical and experimental study of super-radiant systems in the millimeter-wave domain, Phys. Rev. A **27**, 2043 (1983).